Investigation on 3D fatigue crack propagation in surface-cracked specimens

X. Li, H. Yuan,[a)] and J. Y. Sun
Department of Mechanical Engineering, University of Wuppertal, Germany

(Received 17 June 2013; accepted 30 June 2013; published online 10 July 2013)

Abstract In the present work the fatigue crack growth in AISI304 specimens is investigated experimentally. In 3D finite element analysis the virtual crack closure technique is applied to calculate distributions and variations of the stress intensity factor along the surface crack front. It is confirmed that the stress intensity factor along the surface crack front varies non-uniformly with crack growth. Crack growth rate is proportional to the stress intensity factor distribution in the 3D cracked specimen. The fatigue crack growth in surface cracked specimens can be described by the Forman model identified in conventional compact tension specimens. For crack growth in the free specimen surface the arc length seems more suitable to quantify crack progress. Geometry and loading configuration of the surface cracked specimen seem to not affect the fatigue crack growth substantially.
 [doi:10.1063/2.1304102]

Keywords surface crack, crack front, fatigue crack growth, 3D stress intensity factor

Critical cracks exist mainly on surfaces of mechanical components in engineering. To predict fatigue crack growth life, characterization and verification of a surface crack through the conventional fracture mechanics specimen, such as compact tension (CT), are of interesting. From fracture analysis it is known that the stress field in a 3D surface crack differs from the conventional plane strain tip field. The stress intensity factor (SIF) depends additionally on crack front curvature, crack edge to free surface, and structure configuration. Especially, SIF may vary non-proportionally with crack growth. Predictability and accuracy of the fracture mechanics to 3D surface crack are still interesting issue for many mechanical parts under complex loading conditions.

In the present work, surface crack in circular rod of stainless steel AISI304 is studied experimentally. The crack growth rate ($\mathrm{d}a/\mathrm{d}N$) versus stress intensity factor (ΔK) relation with different load ratios (R) was firstly obtained from standard CT specimens. Fatigue crack growth in the CT specimens can be described by the Forman model.[1] To investigate surface crack growth, the axial tension rods are fabricated and pre-cracked. Fatigue crack growth tests on the rods were carried out at different load ratios. Backtracking method[2,3] was attempted for monitoring crack shape evolution. To obtain more accurate SIFs, beach marks on the crack surface were represented by fitting elliptical arc curves. 3D finite element meshes are generated in compliance with the crack configurations. The SIF along the whole crack front was calculated via the virtual crack closure technique (VCCT).[4–7] The relation of crack shape evolution with the SIF distribution along the crack front was discussed. Finally, the Forman model obtained from the standard CT specimen is used to predict the surface crack evolution in tensile rods.

A 3D crack front can be represented by an elliptical arc crack front[8–16] as shown in Fig. 1. Here a denotes the depth of the surface crack. The elliptical crack can be described by the semi-axes, a and b. For a given crack depth, the crack shape can be controlled by the aspect ratio $\alpha = a/b$. For a straight line crack $\alpha = 0$, whereas $\alpha = 1$ represents a part-circular crack.[9,10,14–16] Carpinteri[9] discussed the crack aspect ratio influence on the stress-intensity factor of elliptical-arc crack front. The maximum stress intensity factor is attained correspondence to the deepest point on the crack front in the case of $a/b = 0$, while it is attained near the external surface in the case of $a/b = 1$. Shin and Cai[15] evaluated stress intensity factors along an elliptical surface crack front in a rod using experimental backtracking technique and finite element analysis.

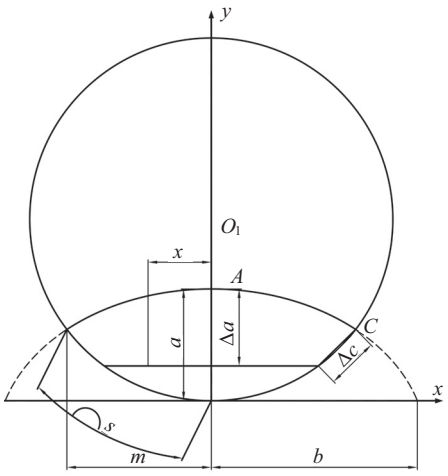

Fig. 1. Comparison between experimental data and prediction of the plasticity model under consideration of the martensite transformation.

For the present specimens, the known solutions can not directly be applied due to arbitrary crack front.

a)Corresponding author. Email: h.yuan@uni-wuppertal.de

The VCCT is widely applied in computing energy release rates based on finite element analysis. The VCCT method provides the energy release rate G_{I} based on the work to be done by the nodal force $F_{y,i}(a)$ against the relative nodal point displacement $\Delta u_{y,i}$ $(a+\Delta a)$ in order to close the crack by Δa.[17] The nodal force $F_{y,i}(a)$ can be obtained from the first step analysis where the crack is closed. The nodal point displacement can be obtained from the second step analysis where the crack has been extended to its full length $a+\Delta a$, as illustrated in Fig. 2.

$$\Delta E_y = \frac{1}{2} F_{y,i}(a) \Delta u_{y,i}(a+\Delta a), \tag{1}$$

$$\Delta G_{\mathrm{I}}^{\mathrm{2D}} = -\frac{\Delta E_y}{t \Delta a}. \tag{2}$$

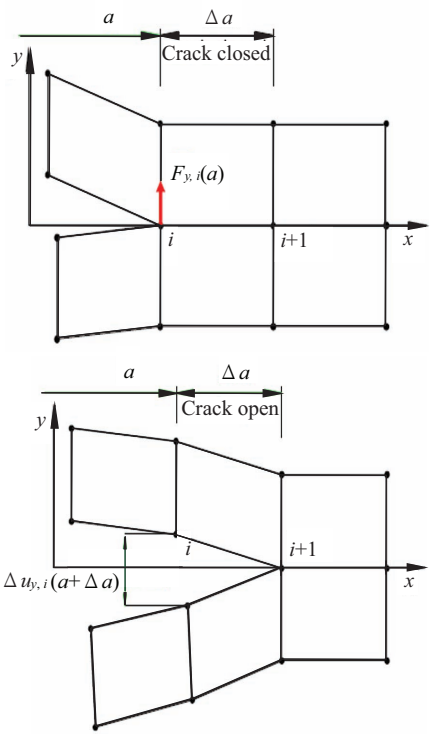

Fig. 2. Illustration of VCCT.

Equation (2) is derived under assumption that the crack front is straight. For an arbitrary shaped crack front the mode definition constantly changes along the counter. A local crack tip coordinate system is necessary to be defined at each nodal point along the front.[18] A half of element and element surface is related to the node in calculation of the energy release rate.

$$K = \sqrt{GE'}, \quad \text{with } E' = \begin{cases} E, & \text{for plane stress,} \\ \dfrac{E}{1-\mu^2}, & \text{for plane strain.} \end{cases} \tag{3}$$

Here, E denotes Young's modulus and μ denotes Poisson's ratio.

Standard CT specimens (50 mm wide and 12.5 mm thick) confirming to ASTM E647 and rod specimens (10 mm in diameter and 138 mm long) are tested. The chemical components of the tested material AISI 304 stainless steel are given in Table. 1. The heat treatment of the raw material is undertaken in vacuum with 1 100°C for one hour and followed by quick cooling in air. The straight-front initial notch was generated in the rod by wire-electrode cutting. The initial flaw depth is taken 1.5 mm for all load ratios.

Table 1. Chemical composition of AISI304

Element	C	Si	Mn	P	S	Cr	Ni
Mass fraction ω	0.040	0.41	1.05	0.035	0.003	17.1	8.1

All tests were performed on MTS 810 servo-hydraulic tension-torsion test machine at room temperature. The CT specimens were tested at the load ratios $R = 0.1, 0.3, 0.5$ with a loading frequency of 15 Hz. The rod specimens were tested at the load ratios $R = 0, 0.1, 0.4$ with a loading frequency of 10 Hz. To reduce the experimental error, two specimens were tested at a given loading condition and the test results show a good repeatability. All specimens were tested under a loading with sinusoidal waveform and in force control.

Instantaneous crack fronts were recorded by creating beach marks using a waveform that the mean load will keep constant but the load amplitude will reduce to 50% for several cycles. By comparing successive crack profiles obtained after loading for designated cycle numbers of each interval, the crack growth rate at different points on the crack front can be evaluated. The crack growth length in CT specimens and the crack depth as well as the surface crack arc length in rod specimens will be measured under light microscope. Figure 3 shows typical beach marked crack surfaces for CT specimen and rod specimen.

A simple and well known method for predicting fatigue crack propagation is a power law described by Paris and Erdogan,[19] and it is also known as Paris law. Forman[20] improved the model by considering effects of K_{C} and stress ratio. Hartman and Schijve[21] proposed the following equations which is the continuation of Formans work by including the threshold stress intensity factor ΔK_{th}

$$\frac{\mathrm{d}a}{\mathrm{d}N} = \frac{C(\Delta K - \Delta K_{\mathrm{th}})^m}{(1-R)K_{\mathrm{C}} - \Delta K}, \tag{4}$$

where C is the intercept and m is the slope on the double logarithmic plot of $\mathrm{d}a/\mathrm{d}N$ versus ΔK. K_{C} is the fracture toughness for the material and ΔK_{th} is the threshold stress intensity factor value for fatigue crack growth which is sensitive to R.

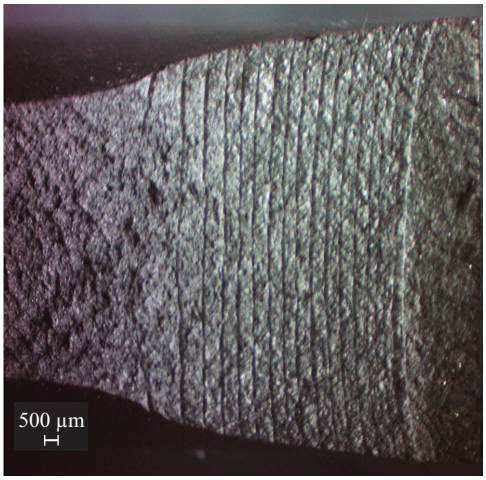

(a)

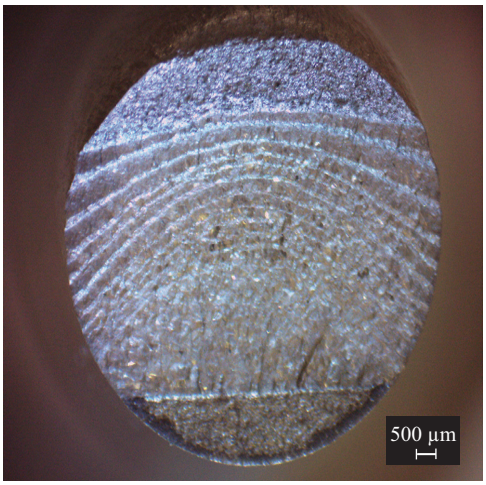

(b)

Fig. 3. Typical beach marked crack surfaces of (a) CT and (b) rod specimen.

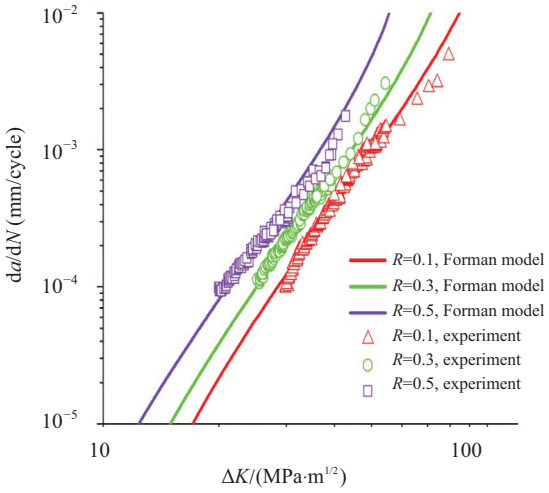

Fig. 4. Crack growth curve of CT specimens.

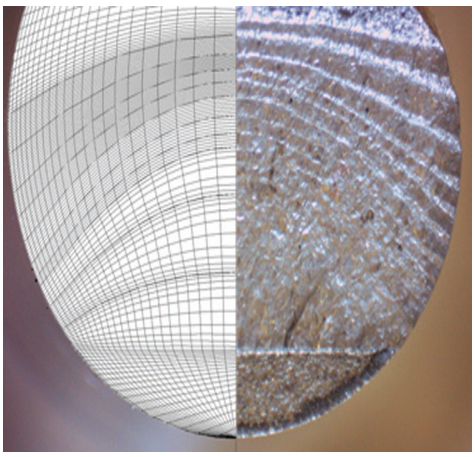

Fig. 5. Element meshes of the cross section in compliance with the crack configurations.

For AISI304 material, the fracture toughness K_{C} is 133 MPa·m$^{1/2}$ and the threshold value ΔK_{th} with $R = 8.053$ MPa·m$^{1/2}$. Fitting with the experimental data, the coefficient can be fixed as $C = 10^{-5.742\,32}$ and $m = 2.801\,92$. The experimental data are shown in Fig. 4 with identified Forman model curves. In the figure the loading ratio effect is clearly illustrated and experimental data agree with the Forman model.

The crack geometry of the rod specimen is described in Fig. 1. An equivalent elliptical arc curve is used to indicate the actual crack front after certain number loading cycles. 3D FE model is generated with symmetric boundary conditions, as shown in Fig. 5. The location of the points on the crack front can be described by the location x/h, with $x = 0$ for the middle of the specimen and $x = h$ for the specimen surface. The crack growth of the deepest point A and the surface point C are represented as the depth length Δa and the chord length Δc, respectively.

From fracture mechanics, the SIF K_{I} for small surface crack can be calculated from

$$K_{\mathrm{I}} = F\sigma\sqrt{\pi a}, \tag{5}$$

where σ is the nominal stress on uncracked ligament, a is the crack depth at point A, and F is the geometry factor. Obviously, F is a function of the crack front geometry and the location. On the other hand, F represents the non-dimensionalized SIF

$$F = \frac{K_{\mathrm{I}}}{\sigma\sqrt{\pi a}}, \tag{6}$$

and can be taken as a variable to characterize distribution of the SIF in the crack front.

To verify the computation of surface crack analysis, the geometry factor F is plotted as a function of the crack depth in Fig. 6(a). The result confirms that VCCT provides reliable results in comparing with other methods.[9,15] In general, the solution by Carpinteri[9] seems higher, whereas Shin[15] agrees with VCCT.

Figure 6(b) shows variations of F along the crack front during crack shape evolution in the rod specimen.

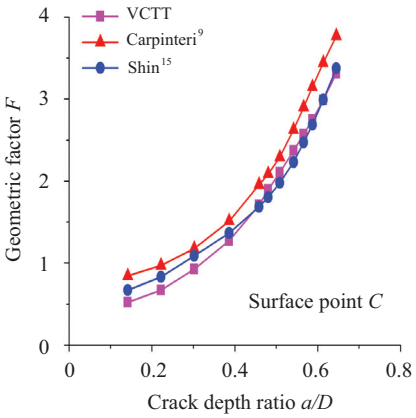

(a) F as a function of crack depth

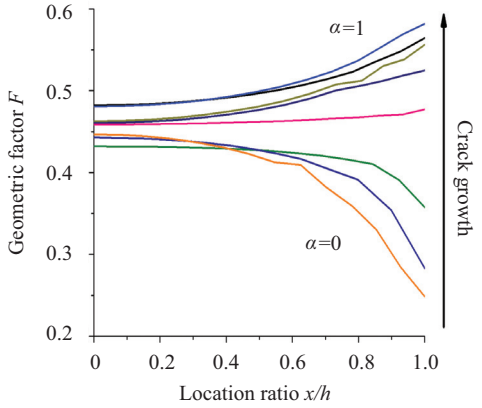

(b) F as a function of crack front

Fig. 6. Element meshes of the cross section in compliance with the crack configurations.

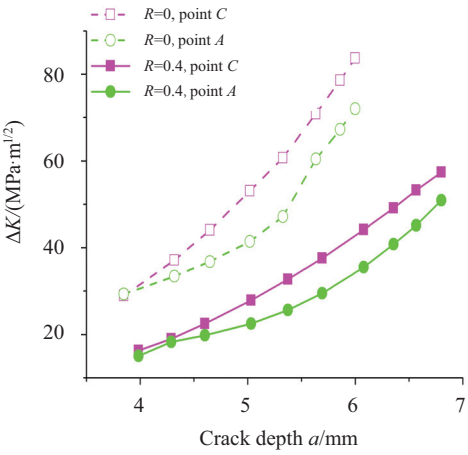

Fig. 7. Development of ΔK in the crack front point A and point C in the cracked rod.

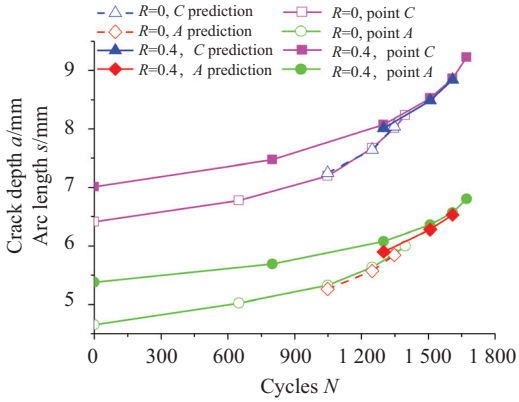

Fig. 8. Crack growth in a surface cracked specimen in fatigue tests.

For the initial notch, a straight crack front with the crack aspect ratio $\alpha = 0$ reveals the maximum SIF in the specimen middle and the SIF decreases with the distance x/h. It implies that the crack propagation starts at point A and the crack front tends to become curved. With the crack developed α increases, the distribution of SIF reaches gradually constant in the whole crack front. In this region the crack front attains a uniform growth rate. Due to varying geometry of the circular rod, the stationary crack growth can not maintain long. The SIF at the crack front near rod surface increases and becomes maximal in the SIF distribution. It follows that the crack propagation near the rod surface is quicker than elsewhere. Variations of the geometry factor F agree with experimental observation, as shown in Fig. 5.

The variations of the geometry factor F can be further found in fatigue crack growth. In Fig. 7, ΔK is plotted as a function of crack growth for points A and C with different loading ratios. Due to transient behavior the crack growth near the initial straight notch is not included in the figure, so that the SIF at point C is mainly larger than that at point A in the whole crack growth process. The curvature of the crack front decreases with crack growth, that is, the crack rate in the middle of the specimen is lower than that near the specimen surface.

The difference of the crack rate can be further observed in Fig. 8, in which the crack length at points A and C is plotted as functions of loading cycles. The predictions are based on the Forman model identified from the CT specimens. The figure shows that the prediction of the Forman model agrees with the experiments well for all investigated loading ratios. Note that the crack length at point A is represented by the crack depth a and the surface point B is given by the arc length s respectively. Fatigue crack growth in the 3D surface cracked specimen can be described by the conventional long crack model.

The crack rate curves for surface crack at points A and C are plotted together with the experimental data for CT specimen in Fig. 9. The Forman model baselines obtained from CT specimens, Eq. (6), are illustrated in the figure. In the range with lower ΔK,

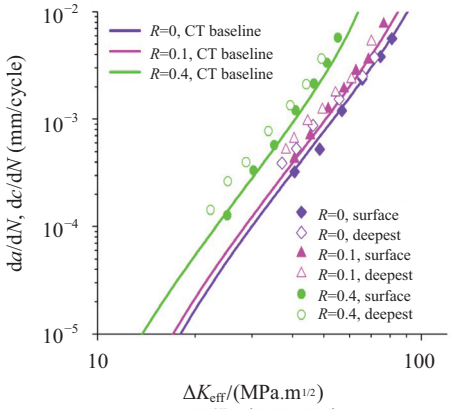

Fig. 9. Crack growth behavior of rod specimen.

the crack growth at the internal crack front is faster than that at the surface point. For high loading range, the crack growth at the surface becomes higher. This phenomenon is also reported by Shin.[15] Generally, the surface crack data agree with the Forman model.

The fatigue crack growth in AISI304 specimens is investigated experimentally. The surface crack in 3D rod under tension is characterized by the fatigue crack data from the CT specimen. 3D finite element models are generated in compliance with the surface crack configurations and the stress intensity factor along the crack front is calculated through virtual crack closure technique. The present work confirms the following facts.

(1) The stress intensity factor along the surface crack front non-uniformly varies with crack growth. Crack growth rate is proportional to the stress intensity factor distribution in the 3D cracked specimen. After crack grows up over the crack front, the maximum of the stress intensity factor appears near the free surface of the tensile rod, so that the crack front curvature becomes smaller.

(2) Experiments confirm that the fatigue crack growth in surface cracked specimens can be described by the Forman model identified in conventional CT specimens. For crack growth in the free specimen surface the arc length seems more suitable to quantify crack progress.

(3) Geometry and loading configuration of the surface cracked specimen seem to not affect the fatigue crack growth substantially. The Forman model can predict local crack front growth rather precisely.

This work was supported by the German Science Foundation(DFG, YU119/5-2).

1. R. G. Forman, V. E. Kearney, and R. M. Engle. Journal of Basic Engineering **89**, 459 (1967).
2. T. L. Mackay and B. J. Alperin, Engineering Fracture Mechanics **21**, 391 (1985).
3. C. S. Shin and C. Q. Cai, International Journal of Fracture **129**, 239 (2004).
4. E. F. Rybicki and M. F. Kanninen, Engineering Fracture Mechanics **9**, 931 (1977).
5. E. F. Rybicki, D. W. Schmueser, and J. Fox, Journal of Composite Materials **11**, 470 (1977).
6. I. S. Raju. Engineering Fracture Mechanics **28**, 251 (1987).
7. F. G. Buchholz, H. Grebner, K. H. Dreyer, et al., *2D- and 3D-applications improved and generalized modified crack closure integral method*, edited by S. N. Atluri and G. Yagawa. *Computational Mechanics'88*, (Springer Verlag, New York, 1988).
8. M. A. Astiz, International Journal of Fracture **31**, 105 (1986).
9. A. Carpinteri, Fatigue & Fracture of Engineering Materials & Structures **15**, 1141 (1992).
10. A. Carpinteri and R. Brighenti, Fatigue & Fracture of Engineering Materials & Structures **19**, 1471 (1996).
11. A. Levan and J. Royer, International Journal of Fracture **61**, 71 (1993).
12. K. D. Thompson and S. D. Sheppard, Engineering Fracture Mechanics **42**, 1019 (1992).
13. K. D. Thompson and S. D. Sheppard, Engineering Fracture Mechanics **43**, 55 (1992).
14. N. Couroneau and J. Royer, International Journal of Fatigue **20**, 711 (1998).
15. C. S. Shin and C. Q. Cai, International Journal of Fracture **129**, 239 (2004).
16. F. P. Yang and Z. B. Kuang, Fatigue & Fracture of Engineering Materials & Structures **30**, 621 (2007).
17. F. G. Buchholz, A. Chergui, and H. A. Richard, *Computational fracture analyses by means of virtual crack closure integral methods*. The 6th Congreso Argentino de Mecanica Computational, Argentina (1999).
18. R. Krueger, Applied Mechanics Reviews **57**, 109 (2004).
19. PC. Paris and F. Erdogan, Journal of Basic Engineering **85**, 528 (1963).
20. R. G. Forman, V. E. Kearney, and R. M. Engle, Journal of Basic Engineering **89**, 459 (1967).
21. A. Hartman and J. Schijve, Engineering Fracture Mechanics **1**, 615 (1970).
22. A. Carpinteri and S. Vantadori, Engineering Materials **378**, 341 (2008).
23. J. Torbio, J. C. Matos, and B. Gonzalez, Engineering Failure Analysis **16**, 618 (2009).
24. J. Torbio, J. C. Matos, B. Gonzalez, et al., Engineering Fracture Mechanics **78**, 3243 (2011).
25. S. Beretta and M. Carboni, Engineering Fracture Mechanics **73**, 2627 (2006).
26. P. Bortot and S. Beretta, *On the estimation of fatigue crack growth in a contaminated H2S environment by interrupted cyclic tests*. Proceedings of the 19th European Conference on Fracture, Russia (2012).